Simulation of Vortex Shedding from a Square Cylinder in Oscillating Channel Flow

Sang Hyun Cho* and Shin-Hyoung Kang**

(Received May 2, 1996)

Laminar vortex shedding of a square cylinder mounted between two parallel walls are numerically simulated by using a finite volunme method based on a linear upwind differencing scheme and SIMPLER algorithm. The unsteady terms are approximated by a two-step fully-implicit backward scheme. The lock-on phenomena in an oscillating flow as well as the vortex shedding in a steady flow are investigated. The values of Strouhal number in the steady uniform flow are reasonably predicted with accuracy by the present numerical method. The frequency range of the incoming flow for the lock-on appear is well simulated. When the flow is loked-on, the shedding frequency is half of the incoming flow frequency. The structural characteristics of shedding vortex in the lock-on range is discussed in the present paper.

Key Words: Vortex Shedding, Lock-on, Oscillation Flow, Finite Volume Method

Nomenclature

C_d : Drag coefficient
C_l : Lift coefficient
U : Time averaged velocity at the inlet
D : Size of square cylinder
H : Channel height
f : Frequency of incoming velocity
f_s : Shedding frequency in oscillating incoming flow
f_{so} : Shedding frequency in steady incoming flow
A : Amplitude of oscillating incoming flow
Re : Reynolds number($=UD/\nu$)
St : Strouhal number($=f_sD/U$)

1. Introduction

Vortex shedding from a bluff body over a wide range of Reynolds number has been an interesting research topic as far as physical aspects and engineering applications are concerned. The vortex flowmeter is one of the applications of the vortex shedding phenomena from the bluff cylinder. Current-generation of vortex flowmeters with high measuring accuracy of one percent of flow rate and wide operating range becomes increasingly popular in industrial process control (Leo, 1991). There are many parameters influencing the performance of the vortex flowmeter and among them the upstream-disturbance is one of the important parameters. Superposition of small amplitudes of pulsations in incoming flow was reported to produce large shift in the characteristic Strouhal number of the meter due to the frequency resonance and to result in large metering errors.

If a bluff cylinder is flexible or flexibly mounted, then resonant oscillation can be excited by the incident flow. The resonance of the vortex shedding and the vibrating frequency is called as lock-on. The lock-on or resonance occurs when the cylinder oscillates in-line with or normal to the incident flow. The lock-on is also observed when a large periodic component is superimposed upon the incident mean flow. The occurrence of the lock-on depends upon the amplitude and frequency for the in-line oscillations or corresponding flow pulsations. There are many sources of disturbance to cause lock-on phenomena, and the review of vortex sheding resonance of bluff bodies was reported by Griffin and Hall (1991)

* Graduate student, Graduate School, Seoul N. University
** Member of KSME, Professor, Dept. of Mechanical Eng., Seoul N. University

Ongoren and Rockwell (1988) visualized symmetric and asymmetric vortex patterns and their competitions over a wide range of oscillation condition of a circular cylinder mounted in the wat channel. Vortex shedding lock-on over a bluff body in a channel has many interesting features to be experimentally and numerically investigated. However, the flow mechanism and its characteristics in the lock-on regime have not sufficiently been understood . In the present study, attention is paid to understand flow the characteristics in the lock-on regime when an incoming velocity oscillates periodically. The laminar vortex shedding and its lock-on over a square cylinder in a channel is numerically simulated. The lock-on phenomena in an oscillating flow as well as the vortex shedding in a steady flow are investigatd. The structural characteristics of shedding vortex in the lock-on range is discussed.

2. Method of Calculation

2.1 Governing equation and boundary conditions

The governing equations for the laminar incompressible flow are the unsteady forms of continuity and Navier-Stokes equations as follows.
Continuity equation:

$$\frac{\partial \rho}{\partial t}+\frac{\partial}{\partial x}(\rho u)+\frac{\partial}{\partial y}(\rho v)=0 \tag{1}$$

Momentum equation:

$$\frac{\partial}{\partial t}(\rho u_i)+\frac{\partial}{\partial x_j}(\rho u_i u_j)=-\frac{\partial p}{\partial x_i}+\mu\frac{\partial^2 u_i}{\partial x_j \partial x_j} \tag{2}$$

The configuration of a square cylinder mounted in the middle of two parallel flat walls is shown in Fig. 1. The size of the square cylinder is D and the height of the channel is H. H/D is varied from 4 to 8, and the case of $H/D=6$ is intensively investigated.

A no-slip condition is used on the channel walls as well as on the cylinder. The locations of the inlet and outlet are fixed -6.5D and 25.5D, respectively from the center of the cylinder, which are the same as the calculations of Davis and Moore (1982).

The parallel flow is assumed at the inlet; uniform or non-uniform. For the oscillating flow, the incoming velocity distribution is given as follow,

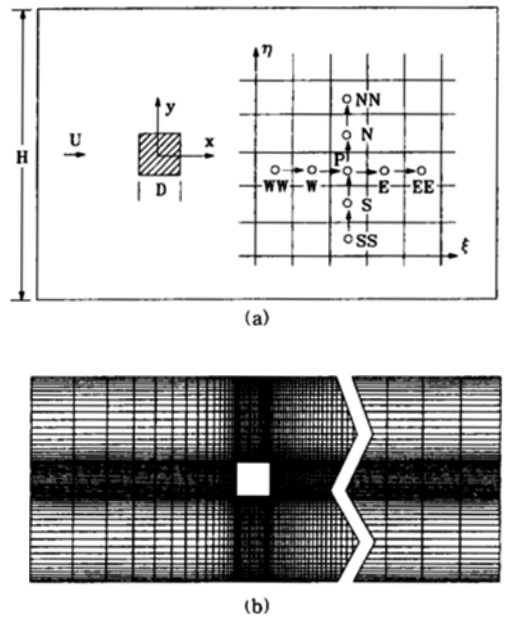

Fig. 1 Coordinate systems and an example of computational domain; (a) coordinate systems, (b) computational domain.

$$u=U[1+A\sin(2\pi ft)] \tag{3}$$

where A is the non-dimensional amplitude and f is the frequency of the oscillating component.

At the exit of the channel, the conventional Neumann condition is not adequate. Davis and Moore (1982) ignored the diffusion terms and employed first-order upwind differencing on the convective terms in the Navier-Stokes equations. Humphrey et al.(1991) used the local flow speed instead of mean velocity at the exit. The convective boundary condition is used in the present calculation, assuming downstream flow doesn't affect the upstream flow.

$$\frac{\partial \alpha}{\partial t}+U_m\frac{\partial \alpha}{\partial x}=0 \tag{4}$$

where U_m and α denote a mean velocity at the exit and a velocity component.

2.2 Method of calculation

A cartesian coordinate system is adopted throught the study. The governing equations are

discretized using a finite volume method with a staggered grid system (Karki, 1986). The pressure is evaluated at the geometric center of the control volume, while the physical convariant velocity components, u_ξ and u_η, are located on the midpoints of the control faces. A linear upwind differencing scheme (LUDS) is employed to evaluate the combined convection-diffusion fluxes on the control surfaces (Peric, 1985). The discretized equation for the scalar variables at a grid point P is written as

$$a_P\phi_P = a_E\phi_E + a_W\phi_W + a_N\phi_N + a_S\phi_S + a_P^n\phi_P^n + a_P^{n-1}\phi_P^{n-1} + b$$
$$a_P = a_E + a_W + a_N + a_S + a_P^n + a_P^{n-1} \quad (5)$$

where the coefficients a's denote the combined convection-diffusion coefficients, and b includes four values of $a_{EE}\phi_{EE}$ etc. as well as explicitly calculated terms. The superscripts n and $n-1$ denote the values at previous two time steps.

The physical covariant velocity components are used as dependent variables in the momentum equations. The discretization is performed using Cartesian velocity components in a locally fixed coordinate system at a grid point P (Karki, 1986). This procedure is reported to avoid complicated curvature source terms which would appear if the full transformation of the equations are used. The discretized equations of the physical covariant velocity components are similar to Eq. (5).

The unsteady terms are approximated using the two-step fully-implicit backward time discretization. Solution for the case of a constant inlet flow field is used for the first initial condition and the solution using the first order time differencing scheme provides the second initial condition.

$$\frac{\partial}{\partial t}(\rho\phi) = \frac{3(\rho\phi)^{n+1} - 4(\rho\phi)^n + (\rho\phi)^{n-1}}{2\Delta t} \quad (6)$$

The method is based on SIMPLER algorithm of Patankar (1980). At each new time step, solution is obtained using an iterative method; i.e. (i) solve a Poisson-type euation for the pressure using the velocity field from the previous iteration, (ii) solve the momentum equations for the velocity components using the pressure field, (iii) solve the pressure correction (continuity) equation and correct the velocity field. A convergence is assumed when the maximum relative error in the pressure field is less than 10^{-4}.

3. Results and Discussions

3.1 Vortex shedding in steady uniform flow

The validity of the present method is investigated simulating the vortex shedding from a square cylinder in the steady uniform flow. For $H/D=6$, the variation of the predicted Strouhal number is tested with different values of the time step, the inlet and outlet locations. The standard values of them are fixed as $\Delta t/T=0.1$, $x/D=-6.5$ and $x/D=25.5$, where T is the convective time scale, D/U. The 96×56 grid points are non-uniformly allocated in the computational domain as shown in Fig. 1. The calculation results were summrized in Table 1.

Suzuki et al.(1993) reported that the grid Reynolds number had a considerable effect on the prediction of Strouhal number. They suggested that of 6.8 $Re_g(=U\Delta x_{min}/\nu)$ was a reasonable value compromising between the required CPU time and the accuracy for $Re_D=150$. The corresponding values of Re_g for $Re_D=1{,}000$ and 200 in the present study are 58.2 and 13.6, respectively. However, the numerical scheme has more influence on the variation of the predicted Strouhal number in the present study and the finer grid is not exercised.

Strouhal numbers are calculated for different values of Reynolds number using the power law difference (PLDS) and linear upwind (2nd order upwing, LUDS) schemes. These results are compared with the measured and calculated

Table 1 Strouhal number variation by calculation, Re=1000 and uniform flow

		St	Reference
Time step	0.5T	0.132	Grid: 96×56
	0.1T	0.140	Inlet: 6.5D
	0.05T	0.140	Outlet: 25.5D
Outlet length	25.5D	0.140	Time step: 0.1T
	40.0D	0.135	Grid: 96×56
			Inlet: 6.5D

results of Davis et al. (1984) in Fig. 2. Since the incoming velocity profile in the experiment is not fully developed nor uniform, two extreme cases of parabolic as well as uniform profiles are assumed here. PLDS considerably underestimates the Strouhal numbers due to its known numerical diffusion error. LUDS is more promising than PLDS for the present problem. Measured values of Strouhal number based on the center-line velocity are located between two calculated values with the parabolic as well as uniform velocity profiles. The inlet velocity profile strongly affects the Strouhal number. The values of Strouhal number at various Reynolds numbers are reasonably predicted in comparison with the predicted

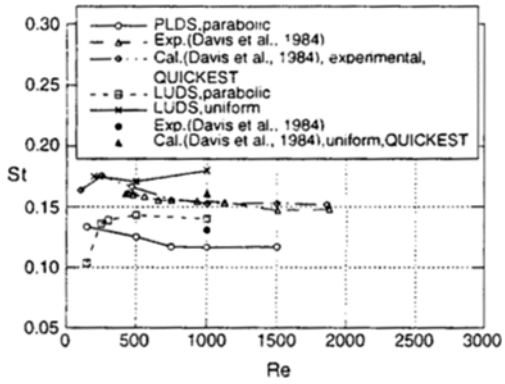

Fig. 2 Strouhal numbers as a function of Re for a square cylinder with steady, uniform inlet velocity: Calculation (Davis, et al., 1984) used experimental velocity profile which was measured in (Davis, et al., 1984).

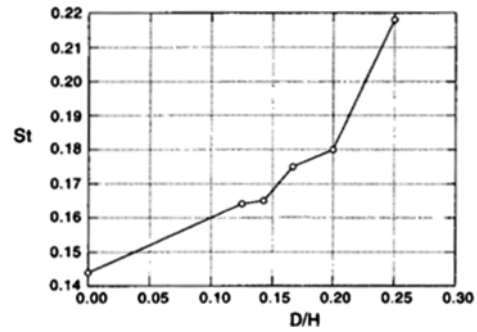

Fig. 3 Variations of Strouhal numbers with various blockage ratios at Re=200 for the steady, uniform inlet velocity.

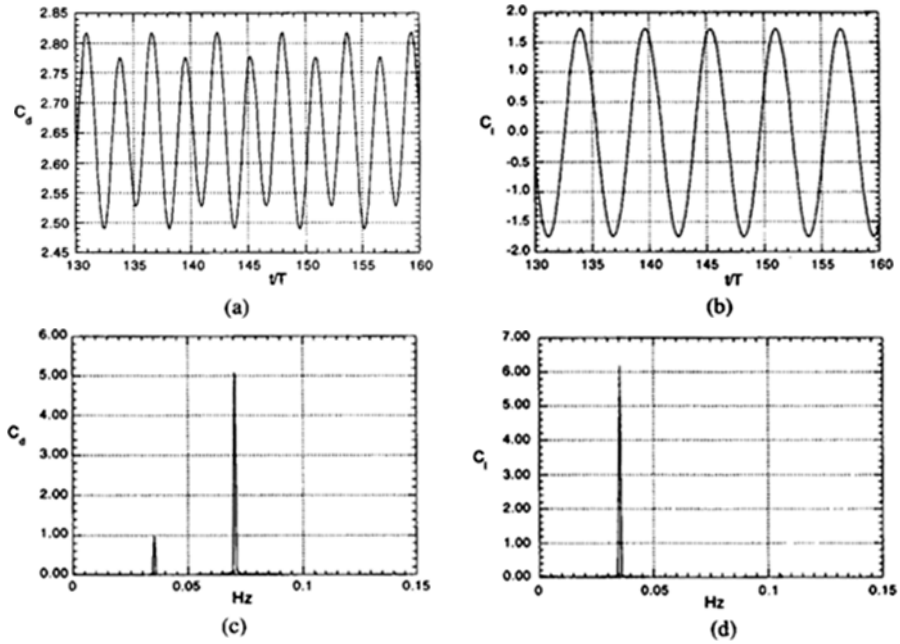

Fig. 4 Instantaneous drag and lift coeffients and their power spectra; (a) drag coefficient, (b) lift coefficient, (c) spectrum of drag, (d) spectrum of lift.

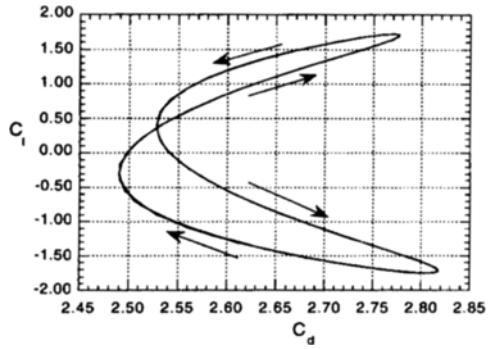

Fig. 5 Phase plot of lift versus drag coefficients.

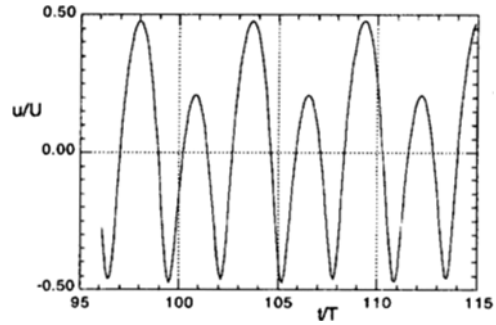

Fig. 6 Instantaneous x-component of velocity at $(x/D, y/D)=(1.483,0.036)$.

and measured values by Davis et al.(1984).

The flows are simulated with several values of H/D to investigate the blockage effect on Strouhal number. The predictied value of Strouhal number of a square cylinder in a uniform free-stream is 0.144 for Re=200. It coincides with the measured value of Okajima (1982) ($0.138<St<0.155$) and the calculated value of Suzuki et al. (1993) (St=0.143 at Re=150). The variation of St with the blockage ratio D/H is shown in Fig. 3. The shedding frequency, i.e. Strouhal number increases as blockage ratio D/H increases. As the blockgae ratio increases, the increase of velocity over the cylider stimulates the interaction of shedding vortex pairs and the frequency increases. However, the vortex shedding, i.e. oscillating and regular motion, disappears when D/H is larger than 2.5.

Hereafter, the details of the flow structure are discussed for the case of $H/D=6$ and Re=200. The variations of drag and lift coefficients and their power spectra are presented in Fig. 4. The drag and lift are obtained by integrating the pressure and viscous stress on the surface of the cylinder. The frequency of the drag is twice that of the lift because the pressure difference between the lower and the upper sides of the cylinder changes once during the pressure difference between the front and the back sides changes twice. The phase plot of the lift versus drag presented in Fig. 5. shows regular and periodic shedding pattern well. The angle of force acting on the cylinder is zero when the magnitude of force is a minimum and the angle is a maximum when it is a maximum as shown in the figure.

The variations of the x-component of veloity at the location $(x/D, y/D)=(1.483, 0.036)$ is shown in Fig. 6. The data acquisition point is located in the strongly rotating flow region and the x-component of veloity has negative values during some time intervals. The variations of drag and x-component velocity at that location shows that a small peak is followed by large one and vice-versa. It is regarded that this phenomenon is caused by the irregularity of the flow. The irregularity of the flow in Humphery et al.(1991) for Re =500 in the infinite flow field was stronger. Their result shows a pattern which is never repeated exactly, although it has a similar segment on the time axis.

Evolution of vorticity contours is presented in Fig. 7. The lower vortex in a strong counter-clockwise rotation at Fig. 7(a) is cut by the upper vertex of clockwise rotation and flows downstream along the upper channel wall. In Fig. 7(b) the next vortex generated at the upper part of the cylinder starts to cut the lower vortex. However, the lower vortex is strong enough to move across the center-line toward the upper wall in Fig. 7(c). The center of the upper vortex moves down to the lower wall and flows downstream because of this effect in Figs. 7(d) and (e), and at the same time other vortices are generated from the lower and upper sides of the cylinder and they make competition. Through the changes shown in Figs. 7(f) and (g), the flow returns the Fig. 7(a) and the

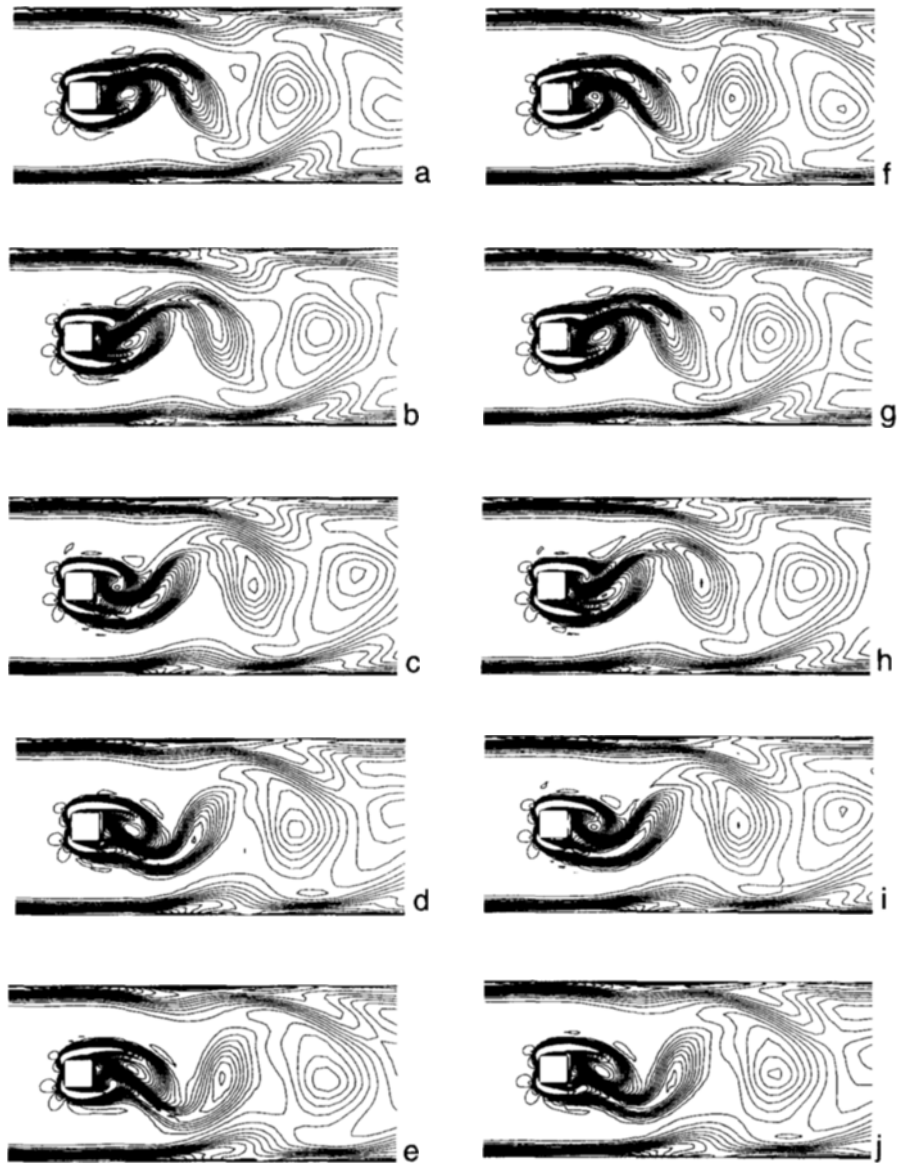

Fig. 7 Evolution of vorticity contours (t/T increases constantly from a to j).

same process of vortex shedding repeats.

3.2 Vortex shedding in oscillating uniform flow

Vortex shedding from the square cylinder with pulsating uniform flow in a channel is simulated. In this case, additional parameters affect the flow, i.e., amplitude and frequency of incoming flow. Barbi et al.(1986) defined the parameter ε considering the similarity of the pulsating flow with the case of in-line oscillation of a cylinder in the unform flow.

$$\varepsilon = UA/2\pi fD \tag{7}$$

ε is the same parameter as a/D for the forced motion of the cylinder, where a denotes the amplitude of the pulsating cylinder. The vortex shedding is simulated for several values of forcing frequency with the value of ε and Reynolds

number fixed (ε=0.173 when Re=1,000 and ε=0.2 when Re=200). The forcing frequency ratio f/f_{s0} is varied from 0.8 to 3.0 for the case of Re=200. f_{s0} is a calculated value for the case of a steady inlet flow. The case of ε=0.2 and Re=200 will be discussed extensively.

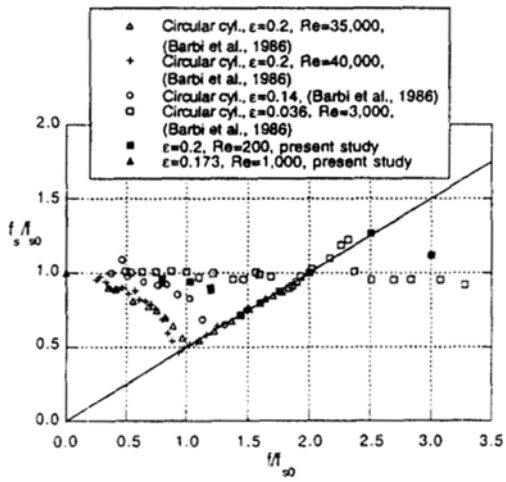

Fig. 8 Variations of f_s/f_{s0} versus f/f_{s0} at Re=200 with oscillating inlet velocity.

The predicted values of shedding frequency are shown in Fig. 8. As the forcing frequency, f increses, the shedding frequency, f_s decreases and locks-on at f/f_{s0}=1.44. The lock-on continues to f/f_{s0}=2.5 and disappears near f/f_{s0}=3.0. In the lock-on regime, the flow field is strongly periodic and the shedding is proportional to the oscillating frequency of the main flow. Outside the lock-on regime the flow has a dominant shedding frequency, but not regular. The phase plots of lift versus drag and the power spectra of the lift coefficient at f/f_{s0}=0.8 and 3.0 are shown in Fig. 9. The calculated lift and drag coeffcients have dominant shedding frequency, but they show several sub-frequencies.

The phase plots of lift versus drag coefficients and the power spectra of lift in the lock-on regime; f/f_{s0}=1.44, 2.0 and 2.5, are shown in Figs. 10, 11 and 12. They are stongly periodic and regular. Each phase plot shows different behavior. The different patterns of phase plot need additional explanation later. The magnitude of the total force acting on the cylinder and the acting angle from the center of the cylinder have

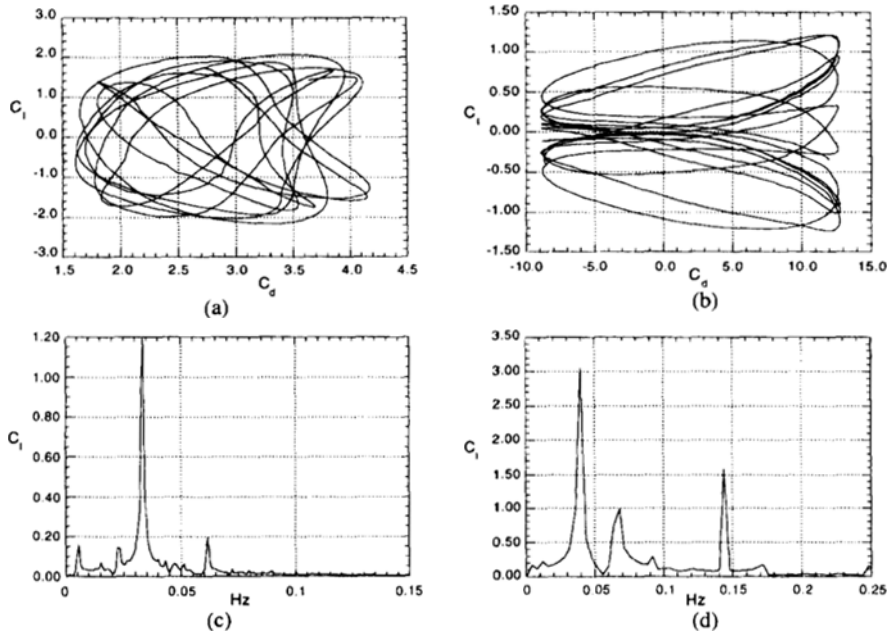

Fig. 9 Phase plots of drag, lift coefficients and power spectra of lift ; (a) phase plot of drag with lift for f/f_{s0} 0.8, (b) phase plot of drag with lift for f/f_{s0}=3.0, (c) spectrum of lift for f/f_{s0}=0.8, (d) spectrum of lift for f/f_{s0}=3.0.

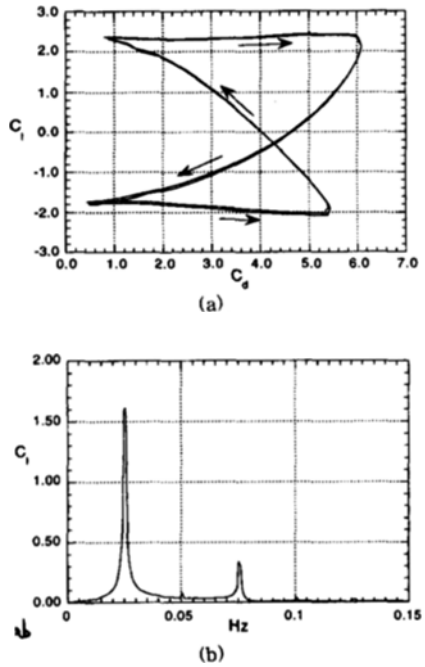

Fig. 10 Phase plot of drag with lift coefficients and a power spectrum of lift for $f/f_{s0}=1.44$: (a) phase plot, (b) spectrum of lift coefficient.

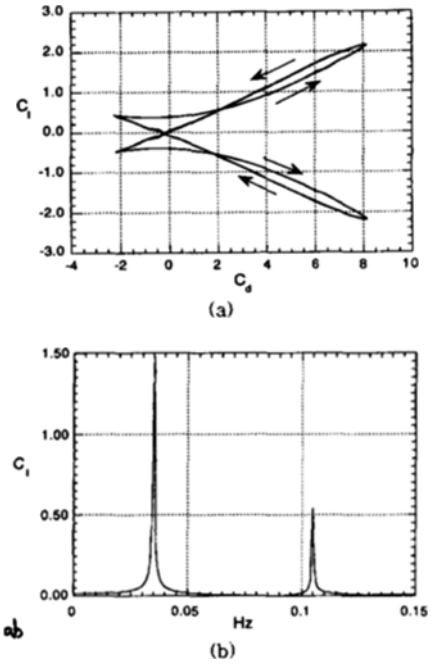

Fig. 11 Phase plot of drag with lift coefficients and a power spectrum of lift for $f/f_{s0}=2.0$: (a) phase plot, (b) spectrum of lift coefficient.

their maxima when the drag is maximum and the lift has the extremum value. The dominant frequency of the drag coincides with the forcing frequency whether f/f_{s0} is in the lock-on regime or not, as indicated by Barby et al.(1986).

The calculated vorticity contours show several aspects of flow patterns. The flow structure in the low freqency is quite similar to that in the steady incoming velocity, however it changes as the frequency increases. The evolution of the vorticity contours for $f/f_{s0}=2.5$, high frequency in the lock-on regime, is shown in Fig. 13. Two vorticies the same sign are shed continuously from the same side of the cylinder in turn. Two shed vortices, i. e. primary and secondary vortex, have different strengths. Chang et al.(1992) mentined that if f/f_{s0} is smaller than 2.0, the primary vortex is stronger than the secondary one and its relation is reversed for the values larger than 2.0. When f/f_{s0} is below 2.0, same results are obtained in the present study, but when f/f_{s0} is above 2.0, the vortices have almost the same strengths. When $f/$

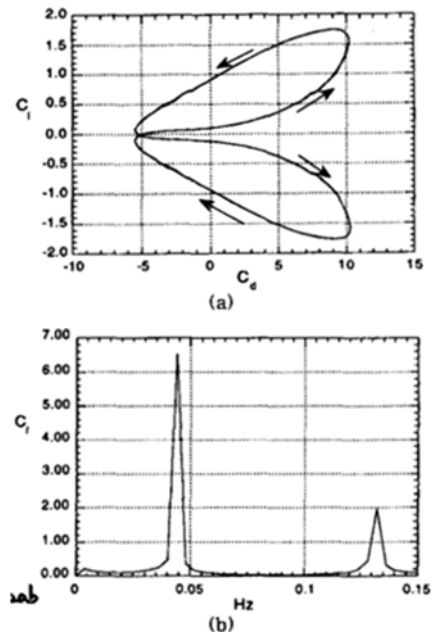

Fig. 12 Phase plot of drag with lift coefficients and a power spectrum of lift for $f/f_{s0}=2.5$: (a) phase plot, (b) spectrum of lift coefficient.

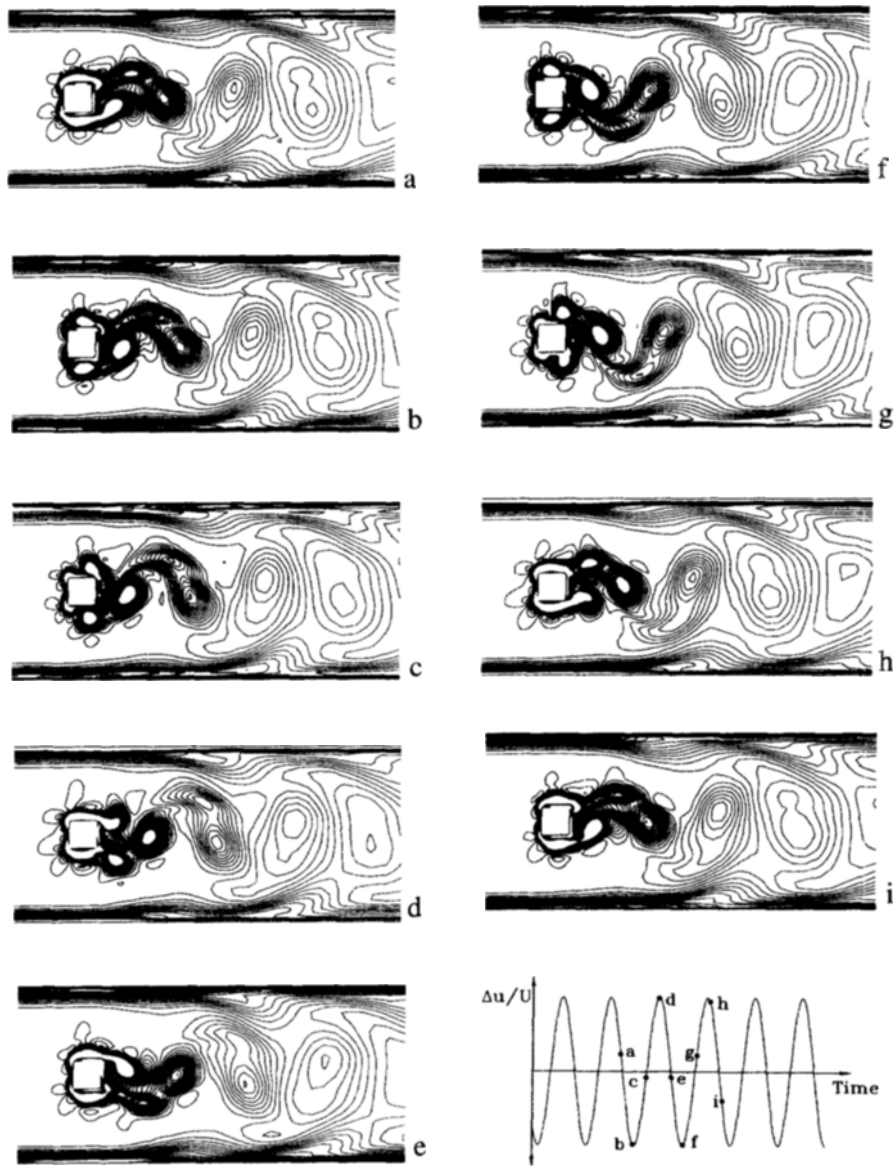

Fig. 13 Evolution of vorticity contours for $f/f_{s0}=2.5$ at Re=200.

f_{s0} is larger than 3.0, the secondary vortex is stronger than the primary one. The primary lower vortex pushes the secondary upper one in Fig. 13(a). A secondary lower vortex and the primary upper one are generated as the incoming velocity is decelerating, and the growing primary lower one cuts the upper vortex in Fig. 13(b). These generated vortices are elongated by the accelerating incoming velocity in Figs. 13(c), (d) and the situation is reversed in Figs. 13(e) to (h). The flow pattern returns to Fig. 13(a) and the whole process repeats. This process explains why the shedding freuency is half of the forcing frequency, i.e. the primary vortex on the one side of cylinder and the secondary one on the other side are generated by a first decelerating velocity and then, the reversed situation is made by the second. The next situation is same as the first. As a result, the

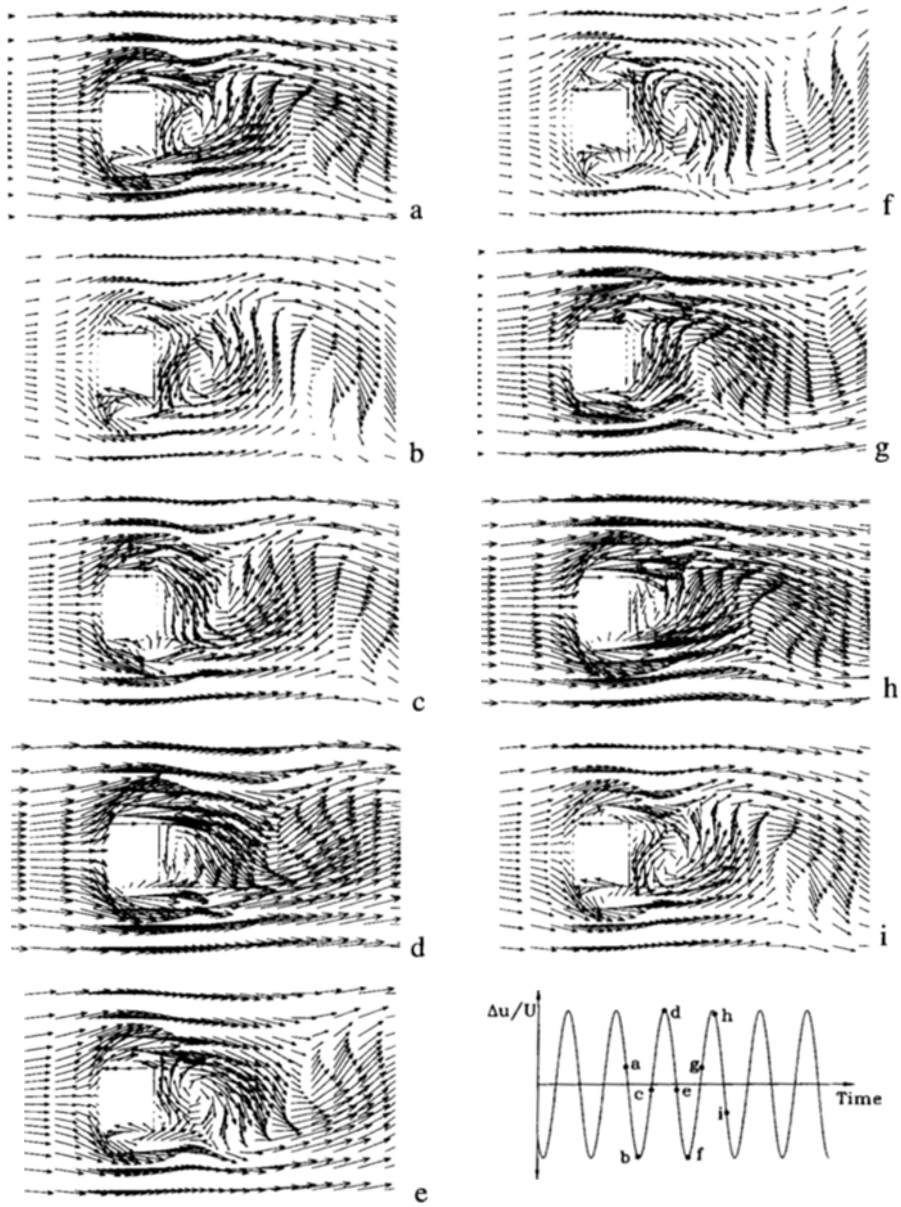

Fig. 14 Evolution of velocity fields for $f/f_{s0}=2.5$ at Re=200.

flow field takes one period while the variation of incoming velocity takes two periods. The whole pattern coincides with the experimental result by Ongoren and Rockwell (1988). They mentioned several vortex shedding patterns when the flow oscillated. Figure 11 coincides with the A-IV mode named by Ongoren and Rockwell (1988).

Negative values of the drag coefficient appear in Fig. 11(a) and Fig. 12(a) in spite of the unchanged flow direction. Negative drag appears from $f/f_{s0}=1.76$ and this phenomenon can be explained using Fig. 14. The value of minimum velocity at the inlet becomes smaller as A increases, which means that the pressure acting on

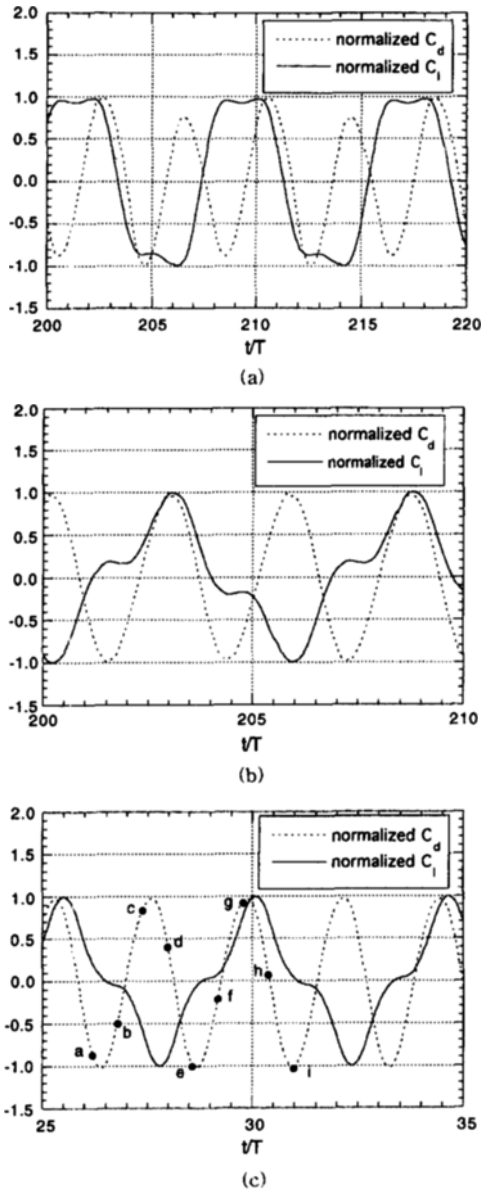

Fig. 15 Instantaneous normalized drag and lift ; (a) $f/f_{so}=1.44$, (b) $f/f_{so}=2.0$, (c) $f/f_{so}=2.5$.

the front side of the cylinder becomes smaller as the inlet velocity decreases. On the other hand, the rotational region behind the cylinder for minimum value of incoming velocity is relatively larger than that for the maximum as can be seen in Figs. 14(b), (d) or (f), (h). The velocity magnitude of the large rotational region is also larger than that of the small one. Because the larger velocity still induces more pressure which acts on the back side of the cylinder, the drag becomes smaller. Therefore, the minimum value of the drag becomes smaller and finally becomes negative as A increases. The inertia of the flow passing the cylinder becomes weak as inlet velocity magnitude is smaller. The rotational region behind the cylinder becomes strong enough to overcome the inertia of the flow over the cylinder and makes back-flow at the upper and lower sides of the cylinder. The back-flow motion makes secondary vortices stronger.

The variations of normalized drag and lift coefficients are shown in Fig. 15. Figure 15 explains why the phase plots of Figs. 10 through 12 are different, i.e. the different lift modes bring about the different phase plot patterns, and vortex competition makes the different lift modes as shown in Fig. 13. The lift in Fig. 15(a) has two peaks in almost same magnitude. They become different as f/f_{so} increases. Finally, there appears only one peak in Fig. 15(c) because the secondary vortex attached on the upper side of cylinder has almost the same strength as the primary one on the lower side as shown in Figs. 13(b) and (f).

Phase difference between the incoming velocity and the drag in the lock-on regime are summarized in Table 2.

Table 2 The phase difference between the incoming velocity and a drag

f/f_{so}	1.44	1.6	1.76	2.0	2.5
Phase difference (degree)	63.6	60.7	66.5	63.0	65.9

The minimum value of the drag in Fig. 15(c) appears between time (a) and (b) in Figs. 14, and the maximum value exists between (c) and (d) in Figs. 14. Pressure acting on the front side of the cylinder increases or decreases as the incoming velocity accelerates or decelerates. However, the time when minimum or maximum drag occurs doesn't coincide with the time when maximum or minimum pressure acts on the front of the cylinder, because of the rotation region behind the cylinder which influences the pressure acting on

the back side of the cylinder as mentioned above. Each phase difference in Table 2 is nearly the same amount. It is thought that all phase differences in Table 2 are due to the time step, Δt, since the peak time of each signal which is extracted from the basic data has an error of Δt.

4. Conclusion

Through the numerical investigation of vortex shedding from a square cylinder in a channel, the results are summarized as follow:

(1) The values of Strouhal number in a steady uniform flow are reasonably predicted using the present numerical method.

(2) The lock-on regime are observed from $f/f_{s0}=$ 1.44 to $f/f_{s0}=2.5$ of the incoming velocity frequency. Drag and lift coefficients in this regime are periodic.

(3) The shedding frequency are half of the forcing frequency because of the secondary vortex which is generated by the oscillating inlet velocity.

(4) A large amplitude of oscillating inlet velocity generates the back-flow motion which make the secondary vortex strong.

(5) The vortex competition makes different patterns of the lift coefficient history in the lock-on regime.

(6) The phase difference between the incoming velocity and the drag exists because the rotational region behind the cylinder influences the pressure acting on the back side of the cylinder, while the pressure acting on the front side varies with change of incoming velocity.

Acknowledgments

The authors appreciate Prof. H. Choi for his advices and comments on the unsteady flow calculations.

References

Arnal, M. P., Goering, D. J. and Humphery, J. A. C., 1991, "Vortex Shedding from a Bluff Body Adjacent to a Plane Sliding Wall," *ASME Journal of Fluids Engineering*, Vol. 113, pp. 384~398.

Barbi, C., Favier, D. P., Maresca, C. A. and Telionis, D. P., 1986, "Vortex Shedding and Lock-On of a Circular Cylinder in Oscillatory Flow," *J. Fluid Mech.*, Vol. 170, pp. 527~544.

Chang, K. S. and Sa, J. Y., 1992, "Patterns of Vortex Shedding from an Oscillating Circular Cylinder," *AIAA Journal*, Vol. 30, No. 5, pp. 1331~1336.

Davis, R. W. and Moore, E. F., 1982, "A Numerical Study of Vortex Shedding from Rectangles," *J. Fluid Mech.*, Vol. 116, pp. 475~506.

Davis, R. W., Moore, E. F. and Purtell, L. P., 1984, "Numerical-Experimental Study of Confined Flow Around Rectangular Cylinders," *Phys. Fluids*, Vol. 27, No. 1, pp. 46~59.

Gruffin, O. M. and Hall, M. S., 1991, "Review-Vortex Shedding Lock-On and Flow Control in Bluff Body Wakes," *ASME Journal of Fluids Engineering*, Vol. 113, pp. 526~537.

Karki, K. C., 1986, "A Calculation Procedure for Viscous Flows at All Speeds in Complex Geometries," Ph. D. Thesis, Univ. of Minnesota.

Leo O'Connor, 1991, "Vortex Meters: High-Accuracy Flow Measurement," *Mechanical Engineering*, Vol. 113, No. 10, October, pp. 46~49.

Ongoren, A. and Rockwell, D., 1988, "Flow Structure from an Oscillating Cylinder. Part Ⅱ: Mode Competition in the Near Wake," *J. Fluid Mech.*, Vol. 191, pp. 225~245.

Okajima, A., 1982, "Strouhal Numbers of Rectangular Cyinders," *J. Fluid Mech.*, Vol. 123, pp. 379~398.

Patankar, S. V., 1980, "Numerical Heat Transfer and Fluid Flow," McGraw-Hill Book Company.

Peric, M., 1985, "A Finite Volume Method for the Prediction of Three-Dimensional Fluid Flow in Complex Ducts," Ph. D. Thesis, Univ. of

London, Imperial College.

Suzuki, H., Inoue, Y., Nishimura, T., Fukutani, K. and Suzuki, K., 1993, "Unsteady Flow in a Channel Obstructed by a Square Rod (crisscross motion of vortex)," *Int. J. Heat and Fluid flow,* Vol. 14, No. 1, pp. 2~9.